Author(s): Nagarajan, S. & Svensk, O. & Lehtola, L. & Lipsanen, Harri & Sopanen, M.

Title: Stress distribution in GaN nanopillars using confocal Raman mapping technique

Year: 2014

Version: Final published version

Please cite the original version:

Nagarajan, S. & Svensk, O. & Lehtola, L. & Lipsanen, Harri & Sopanen, M. 2014. Stress distribution in GaN nanopillars using confocal Raman mapping technique. Applied Physics Letters. Volume 104, Issue 15. P. 151906/1-5. ISSN 0003-6951 (printed). DOI: 10.1063/1.4872056.

AIP | Applied Physics Letters

Stress distribution in GaN nanopillars using confocal Raman mapping technique

S. Nagarajan, O. Svensk, L. Lehtola, H. Lipsanen, and M. Sopanen

Citation: Applied Physics Letters **104**, 151906 (2014); doi: 10.1063/1.4872056
View online: http://dx.doi.org/10.1063/1.4872056
View Table of Contents: http://scitation.aip.org/content/aip/journal/apl/104/15?ver=pdfcov
Published by the AIP Publishing

Stress distribution in GaN nanopillars using confocal Raman mapping technique

S. Nagarajan,[a] O. Svensk, L. Lehtola, H. Lipsanen, and M. Sopanen
Department of Micro and Nanosciences, Aalto University, P.O. Box 13500, FI-00076 Aalto, Finland

(Received 14 February 2014; accepted 7 April 2014; published online 17 April 2014)

In this Letter, high-resolution confocal Raman mapping of stress distribution in etched and re-grown GaN nanopillar structures is investigated. Results of the E_2(high) phonon line mapping of the top surfaces of individual nanopillars reveal differences in stress between both the center and edge of the nanopillar top surfaces and between the etched and re-grown GaN nanopillar structures. In-plane biaxial compressive stress with the values of 0.36–0.42 GPa and 0.49–0.54 GPa is observed at the center of etched and re-grown GaN nanopillars, respectively. The in-plane biaxial compressive stress decreases from center to edge in re-grown GaN nanopillar due to the tilted facets. Also, the A_1(LO) phonon frequency increases from center to edges, or tilted facets, due to the tilt of the c-axis of re-grown GaN nanopillar. © *2014 AIP Publishing LLC*. [http://dx.doi.org/10.1063/1.4872056]

Gallium nitride and its compounds are widely used materials in optoelectronics and power electronics applications due to their wide and tunable band gap, large breakdown field, high carrier mobility, and thermal stability.[1,2] These properties make the material family ideal for devices such as light emitting diodes (LEDs), laser diodes, and high power transistors. Traditional GaN devices rely on lateral layer structures grown by metal organic vapor phase epitaxy (MOVPE) or molecular beam epitaxy (MBE).[3,4] Recently, there has been a lot of interest towards non-lateral GaN nanostructures which might have a huge potential in optoelectronic applications by both improving the efficiency of III-nitride LEDs and modifying the emission spectra of these devices.[5,6] For instance, growth of InGaN/GaN quantum wells on patterned GaN nanopillar structures can be used to achieve polychromatic white light emission due to differences of indium incorporation efficiency and growth rate of different crystal planes.[7] The heteroepitaxial growth of lateral III-nitride layers is subjected to a large residual stress from both thermal and lattice mismatch between the epilayer and the substrate.[8] However, it has been shown that GaN nanopillars and other patterned structures can effectively reduce the strain in the epitaxial layer.[9,10] It has also been proved that the strain relaxation at the surface and sidewalls of the GaN pillars increases the indium incorporation efficiency which opens up possibilities to fabricate more efficient green and yellow LEDs from III-nitride materials.[11] Therefore, it is important to understand the mechanism of strain relaxation in patterned GaN nanopillars. Also, a different dangling bond density and surface energy of different atomic planes can affect indium incorporation efficiency. Previously, strain relaxation in networks of GaN nanopillars has been studied by in-plane x-ray diffraction (XRD) and photoluminescence (PL) measurements.[12,13] However, these studies focused on structures with different nanopillar height and assumed the top diameter to be constant. A finite element method and linear elasticity theory based models have been proposed to understand the strain distribution in individual GaN nanopillars with different aspect ratios and lateral diameters. It is important to remember that the in-plane stress of the nanopillar is not only affected by the height of the pillar but also the lateral diameter and the shape of the pillar cross-section. The in-plane stress also changes immediately when growth is continued on top of the nanopillar templates. In this work, we study the strain distribution in individual GaN nanopillars with different lateral diameters using the confocal Raman mapping technique. In-plane stress of the nanopillars is determined both before and after the regrowth process to see how growth affects the properties of the structure.

The patterning of nanopillar templates was performed on planar 3 μm-thick undoped GaN layers grown by MOVPE on c-plane sapphire substrates using a standard two-step growth process. Trimethyl-gallium (TMGa) and ammonia (NH_3) were used as gallium and nitrogen sources, respectively. For the nanopillar fabrication, a 200 nm-thick silicon dioxide (SiO_2) mask layer was first deposited onto a GaN layer by plasma enhanced vapor phase deposition (PECVD) followed by deposition of a 20 nm-thick nickel (Ni) layer by e-beam evaporation. The Ni/SiO_2/GaN structure was subjected to rapid thermal annealing (RTA) at 850 °C for 2 min in N_2 ambient to form self-assembled Ni islands. The used Ni layer thickness and annealing parameters resulted in elliptically shaped islands with average diameters ranging between 250 and 600 nm. The purpose of the SiO_2 mask was to enhance the island formation and improve the uniformity of the island size and shape. SiO_2 layer also improved the adhesion of the Ni droplets to the sample surface during the etching process steps. The Ni islands together with the SiO_2 layer served as an etch mask to form GaN nanopillars by reactive ion etching (RIE) and inductive couple plasma (ICP) etching. RIE was used to etch through the SiO_2 layer followed by Cl_2/Ar based ICP etching of the GaN layer. The GaN layers were etched down to the thickness of 1 μm resulting in a nanopillar height of 2 μm. The residual Ni mask and SiO_2 were removed by wet etching in aqua regia (3:1 mixture of hydrochloric acid and nitric acid) and diluted hydrofluoric acid (HF) solutions. Before the GaN re-growth on the nanopillar template, the wafers were

[a]E-mail: nagarajan.subramaniyam@aalto.fi

cleaned by piranha etchant and hydrochloric acid (HCl) solution. The GaN re-growth was performed by MOVPE at 1080 °C for 80 s in H_2 ambient with a V/III ratio of 1250. The resultant film thicknesses varied between 40 and 120 nm depending on the crystal plane. During re-growth, the pillar cross-sections are transformed from elliptical to hexagonal due to the diverse growth rates of different crystal planes.[14] Also, as desorption at high temperature H_2 ambient is crystal plane dependent hexagonal pillar formation is further promoted. The re-grown GaN nanopillar has a flat top facet (0001) plane and six smooth tilted facets of hexagonal structure with {1–101} planes (see Fig. 1(c)). Raman mapping analyses were performed on the top of individual etched GaN nanopillars and re-grown GaN nanopillars. The $z(-,-)\bar{z}$backscattering geometry with z parallel to the c-axis was used. In this backscattering geometry, the selection rule for wurtzite structure allows E_2(high) and A_1(LO) phonon scattering. The spectra were acquired at room temperature with a confocal Raman backscattering technique using a 532 nm line from a frequency-doubled Nd:YAG laser for excitation. The laser light was coupled into the microscope using a single-mode fiber and brought on to the sample using a dichroic mirror and a 100× microscope objective (NA 0.9). The spatial resolution is about 300 nm with a spectral resolution of 0.02 cm^{-1}. The measurement tool was focused to get the maximum intensity from the top surface of the pillars which strongly reduces the intensity of the Raman signal from the background of the underlying GaN layer. Also, the measurement depth is about 1 μm as has been determined by laser excitation wavelength, material refractive index, pinhole size, and objective numerical aperture.[15] In the detection beam path, Rayleigh-scattered light was filtered out using an edge filter and a 50 μm core-diameter fiber was used as a confocal pinhole. The backscattered light was then directed to an ultrahigh-throughput spectrometer equipped with an 1800 g/mm grating and thermoelectrically cooled electron-multiplication charge coupled device detector. The XY-positioning of the sample was achieved using a piezoelectric scanning stage, and a stepper motor was used for focus control. The scanning area was 5 μm × 5 μm. The scanning area is divided into 220 lines with 180 measurement points/line.

Figures 1(a) and 1(b) show the top and tilted view scanning electron microscopy (SEM) images of GaN nanopillars after ICP etching and mask removal. The top view of etched GaN nanopillar template shows the pillars have asymmetrical cross-sections which is due to the shape of the Ni nanodroplets used as etch masks. The side walls of the 2 μm-high pillars are nearly vertical with an average side wall angle of 88°. Side walls and the areas between the pillars have some etch induced damage. Figures 1(c) and 1(d) show the top and tilted view SEM images of GaN nanopillars after re-growth using the etched GaN nanopillars as the growth template. The hexagonal geometry is clearly visible after the re-growth. The average diameter (including tilted crystal planes) of an individual pillar is varying from 370 to 860 nm. The angle between tilted sidewall facets and the (0001) plane is measured to be about 61° ± 0.8° which has been associated with {1–101} planes.[7] Insets (a) and (b) of Fig. 2 show the Raman intensity mapping of the etched GaN nanopillar template and the re-grown GaN nanopillar structure, respectively, measured in the range of 500 cm^{-1}–800 cm^{-1} from the same area as shown in the SEM images in Figs. 1(a) and 1(c). The measurement areas are chosen from the edges of the wafers to

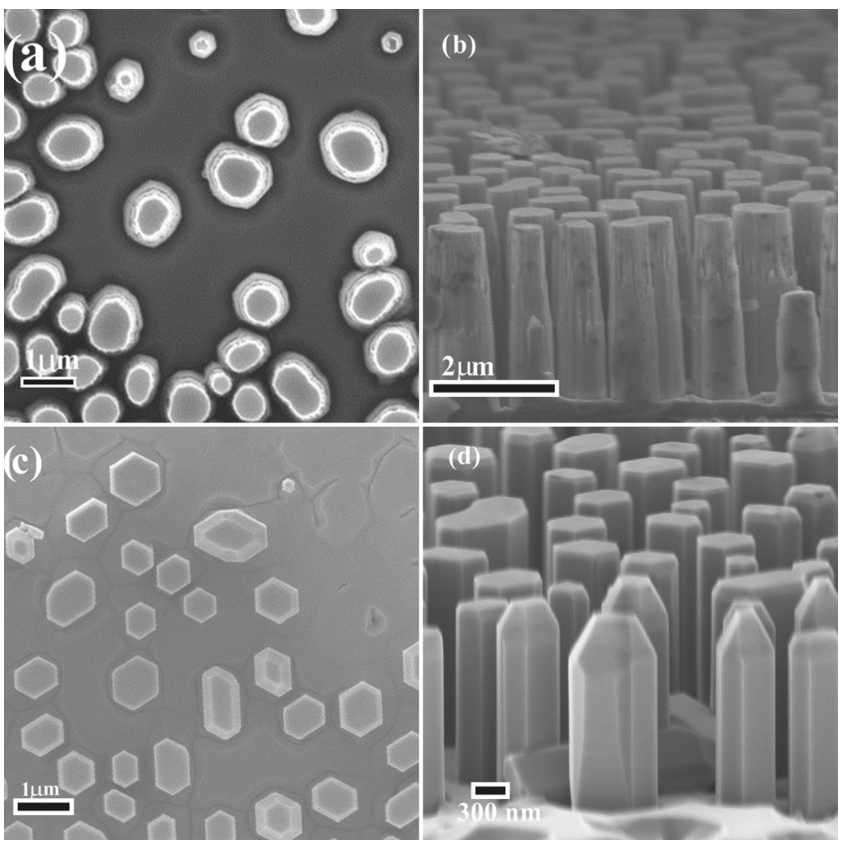

FIG. 1. SEM images of etched GaN nanopillar (a) top view and (b) tilted view. SEM images of re-grown GaN nanopillars (c) top view and (d) tilted view. The scale bar corresponds to 1 μm in (a) and (c), 2 μm in (b) and 300 nm in (d).

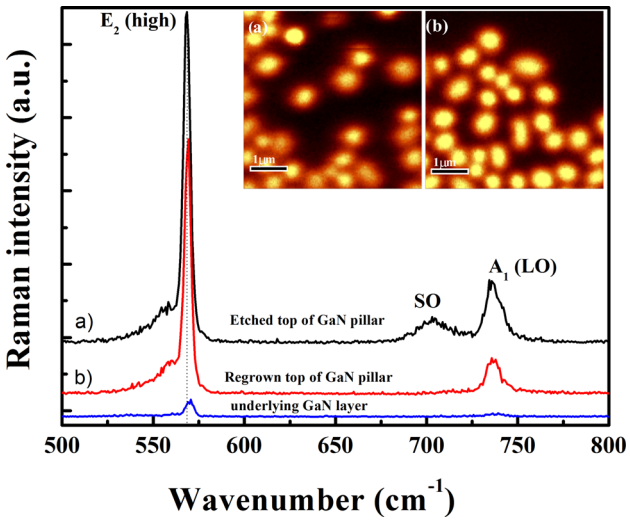

FIG. 2. Raman spectra from a re-grown GaN nanopillar, an etched GaN nanopillar and the underlying GaN layer. The inset shows the Raman intensity mapping of etched and re-grown GaN nanopillar samples measured in the region of 500–800 cm^{-1}. The scale bars in insets correspond to 1 μm.

simplify the detection of the same location in different characterization tools. This explains the rather low density of pillars for some parts of the analysis area. The Raman mapping clearly shows the distribution of the GaN nanopillars on the background GaN surface. The corresponding Raman spectra measured from the top of individual etched and re-grown GaN nanopillars together with the underlying GaN layer are shown in Figure 2. The Raman spectrum of the etched GaN nanopillar reveals a sharp E_2(high) phonon mode at 568.6 cm^{-1} and A_1 (LO) phonon mode at 736.5 cm^{-1}. In addition, there is also a peak located at 703.8 cm^{-1}. Previously, this has been reported as the surface optical (SO) phonon mode in GaN nanostructures.[16] From the re-grown GaN nanopillar, the E_2(high) phonon and A_1 (LO) phonon modes can be observed at 569.3 cm^{-1} and 737.0 cm^{-1}, respectively. The E_2(high) phonon and A_1 (LO) phonon modes of the underlying GaN surface are located at 570.4 cm^{-1} and 738.8 cm^{-1}, respectively. In addition, a weak feature related to the forbidden E_1 (TO) phonon is observed at about 559.0 cm^{-1} from the etched and re-grown GaN nanopillars. The E_2(high) phonon mode is at a higher wavenumber in the re-grown GaN nanopillar and the underlying GaN layer compared to the etched GaN nanopillar. This indicates that the top of the re-grown GaN nanopillar is compressively stressed compared to the top of the etched GaN nanopillar. The intensities of E_2(high) and A_1 (LO) phonons are lower in the underlying GaN layer compared to the etched and re-grown GaN nanopillars due to a slightly out of focus measurement geometry.

To gain more understanding about the stress distribution in individual etched and re-grown GaN nanopillars, a detailed Raman mapping was performed from 563 to 580 cm^{-1} to cover E_2(high) phonon frequencies. In order to obtain the precise E_2(high) phonon frequency position, the measured spectra were fitted with Lorentzian line shapes. Insets of Figs. 3(a) and 3(b) show the Raman image of E_2(high) phonon frequency position fitted with Lorentzian line shape of etched and re-grown GaN nanopillars. Figure 3(a) shows E_2(high) phonon frequency as a function of position (black line) in the area of two etched GaN nanopillars having a different cross-sectional diameter and includes the underlying GaN layer between the pillars. The measurement line is shown in the Raman image in the inset. The frequency profile shows that the maximum of E_2(high) phonon is observed at 569.6 cm^{-1} on the underlying GaN layer. The E_2(high) phonon frequency decreases when moving from the center towards the edges of the GaN nanopillars. The E_2(high) phonon frequency value is strongly dependent on the GaN nanopillar lateral geometry. The E_2(high) phonon frequency value at the center of the pillar top is smaller for smaller cross-sectional diameter GaN nanopillar compared to the larger one. Figure 3(b) shows the

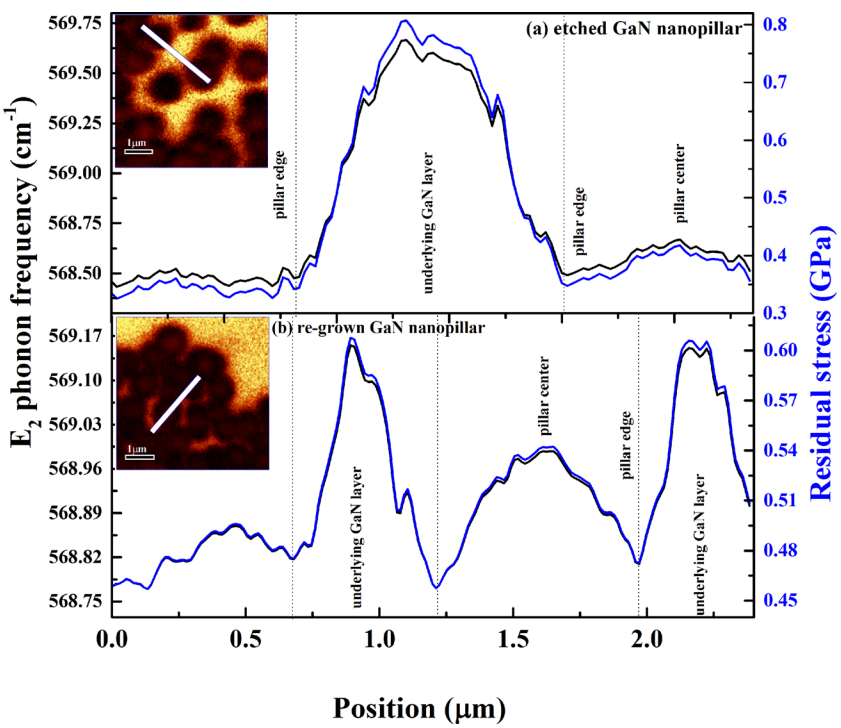

FIG. 3. The inset shows the Raman image of E_2(high) phonon peak position fitted with Lorentzian line shape of GaN nanopillar in the region of 560 cm^{-1}–580 cm^{-1}. Raman frequencies shown in the image are measured along the white lines shown in the insets. Data includes two pillars with different lateral diameters. The corresponding frequency position is shown in black line. The calculated stress is shown in blue line. The scale bars in insets correspond to 1 μm.

E_2(high) phonon frequency profile from two re-grown GaN nanopillars with different lateral sizes and the underlying GaN layer (measured along the line shown in the inset). The maximum of the E_2(high) phonon frequency is located at 569.15 cm^{-1} on the underlying GaN layer. The frequency minimum (568.8 cm^{-1}) is located at the edges of the hexagonal nanopillars, and it does not have a clear correlation with the pillar diameter. The frequency at the center of the pillar is heavily dependent on the average pillar diameter and increases from 568.85 cm^{-1} to 568.98 cm^{-1} when pillar diameter increases from 380 nm to 620 nm. The relation between E_2(high) phonon frequency shift and the residual stress is given by[17] $\Delta\omega(cm^{-1}) = \omega - \omega_0 = K\Delta\sigma$, where ω and ω_0 are the E_2(high) phonon frequencies of measured structure and a strain free thick GaN layer (567.6 cm^{-1}), respectively. K (cm^{-1}/GPa) is a proportionality constant and equals to 2.56 cm^{-1}/GPa.[18] $\Delta\sigma = \sigma_{xx} + \sigma_{yy}$ is the in-plane biaxial compressive stress. The calculated residual stress values of the nanopillar top surfaces together with the underlying GaN layers are plotted in blue color in Figures 3(a) and 3(b). Results show that the biaxial compressive stress distribution is heavily dependent on the lateral dimension of the GaN nanopillar. However, the maximum stress is observed at the underlying GaN layer with a value of about 0.70 ± 0.1 GPa. The stress in the underlying GaN surface depends on the amount and size of nanopillars next to the measurement location. If the exposed area between the pillars is relatively large, the stress is higher (about 0.8 GPa) and if the two pillars are very close to each other the stress between the pillars is about 0.6 GPa. Analysis did not reveal any clear difference in the stress of the underlying GaN between the etched and re-grown surface. When full width at half maximum (FWHM) values of E_2(high) phonon frequencies of the etched and re-grown underlying GaN layers were compared (not shown here), the ICP etch damage was seen as a larger FWHM value of 6.9 cm^{-1} in the etched surface compared to a 5.1 cm^{-1} in the re-grown surface. It is also evident that the stress is higher in the center than at the edge of both etched and re-grown GaN nanopillars. The maximum biaxial compressive stress is about 0.36–0.42 GPa in the center of the etched GaN nanopillars and 0.49–0.54 GPa in the center of the re-grown GaN nanopillars (depending on a top diameter). Figure 4 shows the residual stress at the center of the etched and re-grown GaN nanopillars as a function of pillar diameter from 200 to 650 nm. It is evident that the stress in the middle (0001) plane of the nanopillar increases as soon as re-growth process is started. The average difference of the biaxial compressive stress is about 0.1 GPa for etched and re-grown GaN nanopillars with the same lateral diameter. The increase of stress in the re-grown GaN nanopillar compared to the etched GaN nanopillar may be related to etch induced damage releasing the stress inside the pillar. The FWHM of the E_2(high) phonon line at the middle of an etched and a re-grown GaN nanopillar was also compared. The FWHM value of about 4.7 cm^{-1} in the re-grown GaN nanopillar shows higher crystalline quality compared to the value of 5.1 cm^{-1} measured in the etched GaN nanopillar. During re-growth, the overall crystal quality of the pillar is improved, resulting in higher compressive stress in the pillar. In previous studies, a finite element method and continuous media approach have shown that the in-plane stress is sensitive to the geometry and aspect ratio of the nanopillars.[12,13] It has been shown that the part more accessible to the free surface is more flexible to release strain. Recently, Le Boulbar *et al.* have studied the strain relaxation of etched and re-grown GaN nanorods using Raman spectroscopy.[19] They show that the GaN nanorods are fully relaxed in etched and re-grown structures. Re-growth of GaN onto the etched nanorods does not re-introduce strain in their studies. However, in our case, with the confocal Raman mapping technique, we are able to experimentally determine the stress distribution at the surface of the individual nanopillars with different diameters and surface geometries. Based on our results, the stress in the re-grown GaN nanopillar depends strongly on the geometry.

In order to understand the biaxial compressive stress relaxation from the center to the edges, or tilted facets, of re-grown GaN nanopillars, we have performed A_1(LO) phonon mapping. The inset of Figure 4(b) shows the Raman image of the A_1 (LO) phonon frequency position fitted with

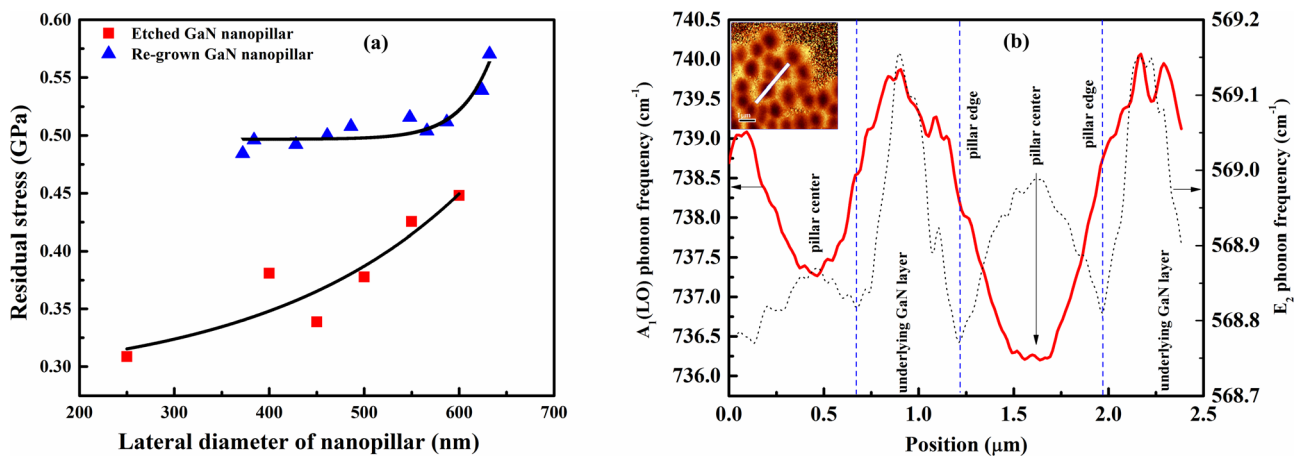

FIG. 4. (a). Residual stress of etched and re-grown GaN nanopillars with varying lateral diameter. Figure 4(b) The inset shows the Raman image of A_1(LO) phonon peak position fitted with Gaussian line shape of GaN nanopillar in the region of 720 cm^{-1}–750 cm^{-1}. Raman frequencies shown in the image are measured along the white line shown in the inset. Data includes two pillars with different lateral diameters. The corresponding peak position is shown in red line. E_2(high) phonon frequency position in the same area is shown for comparison in dotted line. The scale bar in the inset of Raman image corresponds to 1 μm.

Gaussian line shape from 720 cm^{-1} to 750 cm^{-1}.The corresponding peak position is shown with the red line. Also, the E_2(high) frequency position is shown in dotted line for comparison. The A_1(LO) phonon position and E_2(high) phonon line positions show a clear relation. A_1(LO) phonon frequency is observed at about 736 ± 1.02 cm^{-1} at the center of the top of the GaN nanopillars having different diameters of 380 nm and 620 nm. This indicates that the center of the top of the re-grown GaN nanopillar is along the (0001) axis. Moreover, the A_1(LO) phonon frequency shifts to higher wavenumbers when moving from the center to the tilted facets of the GaN nanopillars. On the other hand, A_1(LO) phonon frequency is observed at about 740 cm^{-1} from the underlying GaN layer. Previously, the shifting of A_1(LO) phonon position towards the E_1(LO) phonon position has been reported as quasilongitudinal (QLO) modes due to the tilting of crystal axes relative to the phonon propagation direction.[20] The intermediate energies of the QLO mode between the A_1(LO) and E_1(LO) phonon mode can be calculated using[21] $\omega^2_{QLO}(LO) = \omega^2_{A1(LO)}\cos^2(\theta) + \omega^2_{E1(LO)}\sin^2(\theta)$, where θ is the angle between the phonon propagation direction and the c-axis of the sample. The LO phonon has a frequency between that of the A_1(LO) mode (phonon propagation along the c-axis, θ is equal to 0°) and that of E_1(LO) phonon mode (θ is equal to 90°). The phonon propagation at the center of top of GaN nanopillar is about 736 ± 1.02 cm^{-1} meaning that this has (0001) axis. On the other hand, the shifting of A_1(LO) phonon to higher wavenumbers when moving from center to the tilted facets of the GaN nanopillars is due to light refraction away from normal incidence.[20] Furthermore, as ICP processing etches uniformly the GaN layer, the underlying GaN layer (not covered by Ni) area becomes very rough due to ion bombardment. The bombardment of energetic ions during dry etching accelerates the atom removal at the layer surface and introduces ion induced damages, deteriorating the crystalline quality. This roughened underlying GaN layer thus scatters the light from the normal incidence which in turn shifts the polar-sensitive A_1(LO) to a higher wavenumber.[22] The material under the tilted facets of the pillars is grown in both the lateral and vertical (0001) growth directions during the re-growth process. The crystal quality in this area is very high due to homoepitaxial growth. Therefore, the mechanism of stress relaxation when moving from center to edge in the re-grown GaN nanopillars is due to the growth direction. On the other hand, etching induced damage and dislocations may cause increased stress relaxation when moving from center to edges in the etched GaN nanopillars. Moreover, the part more accessible to the free surface area causes stress relaxation in both etched and re-grown GaN nanopillar.

In summary, the stress distribution of individual etched and re-grown GaN nanopillars have been studied by confocal Raman mapping. The biaxial compressive stress in etched and re-grown GaN nanopillars is shown to strongly depend on the nanostructure geometry. The stress relaxation is observed when moving from center to edge in both the etched and re-grown GaN nanopillars. In the re-grown GaN nanopillar, the stress relaxation from center to edge is attributed to the tilted facets. The A_1(LO) phonon shifts to a higher wavenumber, due to light refraction in the tilted facets of re-grown GaN nanopillar, which supports the stress relaxation mechanism.

This work was supported by the Academy of Finland through Project No. 13256332.

[1]H. Amano, N. Sasaki, I. Akasaki, and Y. Toyoda, Appl. Phys. Lett. **48**, 353 (1986).
[2]S. Nakamura, Jpn. J. Appl. Phys., Part 2 **30**, L1705 (1991).
[3]I. Akasaki, H. Amano, Y. Koide, K. Hiramatsu, and N. Sawaki, J. Cryst. Growth **98**, 209 (1989).
[4]Y. Kim, G. S. Sudhir, H. Siegle, J. Kruger, P. Perlin, E. R. Weber, S. Ruvimov, and Z. Liliental-Weber, J. Appl. Phys. **88**, 6032 (2000).
[5]D. W. Lin, C. Y. Lee, C. Y. Liu, H. V. Han, Y. P. Lan, C. C. Lin, G. C. Chi, and H. C. Kuo, Appl. Phys. Lett. **101**, 233104 (2012).
[6]Y. Kawakami, A. Kaneta, L. Su, Y. Zhu, K. Okamoto, M. Funato, A. Kikuchi, and K. Kishino, J. Appl. Phys. **107**, 023522 (2010).
[7]Z. Fang, Nanotechnology **22**, 315706 (2011).
[8]S. Choi, E. Heller, D. Dorsey, R. Vetury, and S. Graham, J. Appl. Phys. **113**, 093510 (2013).
[9]P. Yu, C. H. Chiu, Y. R. Wu, H. H. Yen, J. R. Chen, C. C. Kao, H. W. Yang, H. C. Kuo, T. C. Lu, W. Y. Yeh, and S. C. Wang, Appl. Phys. Lett. **93**, 081110 (2008).
[10]S. Nagarajan, O. Svensk, M. Ali, G. Naresh-Kumar, C. T. Cowan, S. Suihkonen, M. Sopanen, and H. Lipsanen, Appl. Phys. Lett. **103**, 012102 (2013).
[11]Y. H. Ra, R. Navamathavan, J. H. Park, and C. R. Lee, Nano Lett. **13**, 3506 (2013).
[12]W. J. Tseng, M. Gonzalez, L. Dillemans, K. Cheng, S. J. Jiang, P. M. Vereecken, G. Borghs, and R. R. Lieten, Appl. Phys. Lett. **101**, 253102 (2012).
[13]M. Hugues, P. A. Shields, F. Sacconi, M. Mexis, M. A. Maur, M. Cooke, M. Dineen, A. D. Carlo, D. W. E. Allsopp, and J. Z. Perez, J. Appl. Phys. **114**, 084307 (2013).
[14]J. R. Chang, S. P. Chang, Y. J. Li, Y. J. Cheng, K. P. Sou, J. K. Huang, H. C. Kuo, and C. Y. Chang, Appl. Phys. Lett. **100**, 261103 (2012).
[15]W. L. Chen, Y. Y. Lee, C. Y. Chang, H. M. Huang, T. C. Lu, and Y. M. Chang, Rev. Sci. Instrum. **84**, 113108 (2013).
[16]J. H. Zhu, J. Q. Ning, C. C. Zheng, S. J. Xu, S. M. Zhang, and H. Yang, Appl. Phys. Lett. **99**, 113115 (2011).
[17]C. Kisielowski, J. Kruger, S. Ruvimov, T. Suski, J. W. Ager III, E. Jones, Z. Liliental-Weber, M. Rubin, and E. R. Weber, Phys. Rev. B **54**, 17745 (1996).
[18]J. W. Wagner and F. Bechstedt, Appl. Phys. Lett. **77**, 346 (2000).
[19]E. D. L. Boulbar, I. Girgel, C. J. Lewins, P. R. Edwards, R. W. Martin, A. Satka, D. W. E. Allsopp, and P. A. Shields, J. Appl. Phys. **114**, 094302 (2013).
[20]F. Demangeot, J. Gleize, J. Frandon, M. A. Renucci, M. Kuball, D. Peyrade, L. M. Ferlazzo, Y. Chen, and N. Grandjean, J. Appl. Phys. **91**, 2866 (2002).
[21]R. Loudan, Adv. Phys. **13**, 423 (1964).
[22]T. L. Williamson, D. J. Diaz, P. W. Bohn, and R. J. Molnar, J. Vac. Sci. Technol. B **22**, 925 (2004).